Charge ordering and structural distortions at low temperature in $La_{2-2x}Sr_{1+2x}Mn_2O_7$ ($x=0.475$ and 0.5)

S. B. Wilkins,* P. D. Spencer, T. A. W. Beale, and P. D. Hatton†
Department of Physics, University of Durham, Rochester Building, South Road, Durham DH1 3LE, United Kingdom

M. v. Zimmermann
Hamburger Synchrotronstralunglabor (HASYLAB) at Deutsches Elektronen Synchrotron (DESY), Notkestrasse 85, 22603 Hamburg, Germany

S. D. Brown
XMaS CRG, European Synchrotron Radiation Facility, Boîte Postale 220, 38043 Grenoble Cedex, France

D. Prabhakaran and A. T. Boothroyd
Department of Physics, University of Oxford, Clarendon Laboratory, Parks Road, Oxford OX1 3PU, United Kingdom
(Received 16 September 2002; revised manuscript received 10 January 2003; published 30 May 2003)

In this paper we present x-ray scattering results of charge and orbital ordering in the bilayer manganite $La_{2-2x}Sr_{1+2x}Mn_2O_7$ with doping levels $x=0.5$ and $x=0.475$. Using high-energy x-ray scattering, the structural modulation due to the Jahn-Teller ordering and the charge ordering due to the Mn^{3+}/Mn^{4+} pattern have been measured. Both the $x=0.5$ and $x=0.475$ samples are found to display charge and Jahn-Teller order. We have confirmed that the wave vectors of the Jahn-Teller order, charge order, and orbital order are $\vec{Q}=(0.25,0.25,0)$, $\vec{Q}=(0.5,0.5,0)$ and $\vec{Q}=(0.25,0.25,0)$. The origin of these has been confirmed by resonant x-ray scattering in the vicinity of the Mn K edge using polarization analysis. Contrary to previous studies, the Jahn-Teller order is found to be not reentrant, but is found to reduce in intensity at temperatures below 140 K for both samples. Charge ordering was also detected in the $x=0.5$ sample below this temperature.

DOI: 10.1103/PhysRevB.67.205110 PACS number(s): 61.10.Nz, 71.27.+a, 71.30.+h, 75.47.Gk

I. INTRODUCTION

The hole-doped $3d$ transition-metal oxides have been studied extensively over the past few years due to their remarkable physical properties; the most interesting being the high-temperature superconductivity displayed by the cuprates[1] and the colossal magnetoresistance (CMR) shown by the manganites.[2] The three-dimensional half-doped perovskite manganite systems have been studied intensely in order to investigate the relationship between the charge, spin, structural and orbital degrees of freedom. The electronic and magnetic properties have been studied in an effort to achieve an understanding of the mechanism associated with the CMR behavior. Neutron-, electron-, and x-ray-diffraction techniques have allowed the behavior of the charge, spin, and structural properties to be investigated thoroughly, and recently it has also been possible to investigate the behavior of the orbital degree of freedom using resonant x-ray scattering techniques.[3,4] However, more work is needed to understand the relationship of orbital ordering with the other degrees of freedom in the system and the electronic and magnetic properties.

The magnetoresistive properties are very sensitive to the dimensionality of the manganese oxide lattice, and by inserting rock salt layers between manganese oxide sheets it is possible to dramatically vary the electronic and magnetic properties of the system. This group of compounds are known as the Ruddlesden-Popper series, and they have the general formula $(La, Sr)_{n+1}Mn_nO_{3n+1}$ where n is an integer. The $n=1$ single-layered perovskite $La_{0.5}Sr_{1.5}MnO_4$ shows no metallic or ferromagnetic state,[5] while the $n=\infty$, which corresponds to the cubic perovskite structure, shows the CMR effect.[6] By varying the value of n, the properties of the system are dramatically changed, and they should eventually approach those of the cubic system as n is increased towards infinity.

The bilayer system, as shown in Fig. 1, has the $I4/mmm$ tetragonal space group lattice parameters with $a=b\simeq 3.87$ Å and $c\simeq 20$ Å. The presence of the rock salt blocker layer has the effect of reducing the dimensionality, and in the $x=0.4$ doped system there exists a paramagnetic-to-ferromagnetic transition at 126 K with a huge accompanying change in the CMR.[7]

By changing the ratio of lanthanum to strontium, holes are doped into the system, and this changes the electronic and magnetic properties. For the half-doped bi-layer system the structure within the a-b plane is the same as that in the half-doped three-dimensional (3D) manganites and the single-layered $n=1$ manganite. The bilayer system would therefore be expected to display the same charge/orbital order checkerboard state seen in the 3D manganites, which was predicted by Goodenough in the 1950s.[8] A schematic of the proposed ordering of the manganese ions at a height of $z\sim 0.1$ and ~ 0.9 is shown in Fig. 2. The manganese ions at heights of $z\sim 0.4$ and ~ 0.6 are similarly ordered, but with an origin shift of (0.5, 0.5, 0). The bilayer system is often indexed with $a=b=a_p$ as opposed to the 3D systems where it is indexed with $a=b\approx 2\sqrt{a_p}$. This corresponds to a rotation of the a and b axes by 45°, and in this model the superlattice

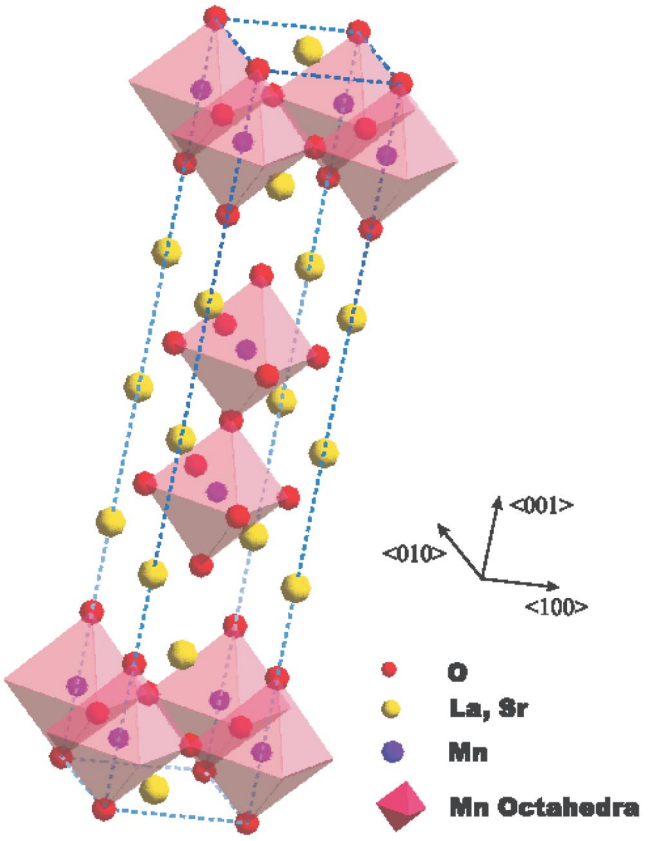

FIG. 1. Diagram showing the crystal structure of the bilayer manganite $La_{2-2x}Sr_{1+2x}Mn_2O_7$.

reflections should occur at modulations of $Q_{CO}=(0.5,0.5,0)$ and $Q_{OO}=(0.25,0.25,0)$ for the charge and orbital order, respectively. The true orbital order supercell is smaller than that shown in Fig. 2 with space group *Amam*. However, we have chosen to use the larger supercell in order to be consistent with the previous literature. This pattern has been found in the 3D manganites $Nd_{0.5}Sr_{0.5}MnO_3$,[9] $Pr_{0.5}Ca_{0.5}MnO_3$,[10] and in the layered type perovskite $La_{0.5}Sr_{1.5}MnO_4$.[3]

Electron[11,12] and x-ray-diffraction studies[13] have shown the presence of a charge and orbitally ordered state at low temperatures. In the electron-diffraction measurements by Li *et al.*[11] and Kimura *et al.*,[12] the appearance of charge order reflections at (0.25, 0.25, 0) around the Bragg peaks below 220 K was reported, and that they maximize in intensity at approximately 180 K before disappearing at 100 K. In addition, x-ray-diffraction studies have been performed using resonant x-ray scattering and high-energy x-ray scattering.[13,14]

Among the x-ray and electron-diffraction measurements, there has been some disagreement in the position of the charge, Jahn-Teller, and orbital order satellites in the literature. The electron diffraction measurements by Kimura *et al.*[12] and the high-energy measurements of Chatterji *et al.* reported that the charge order satellites occurring at a modulation of (0.25, 0.25, 0) around the Bragg peaks. However, the resonant measurements carried out by Wakabayashi *et al.*[14] have reported the charge order at a modulation of

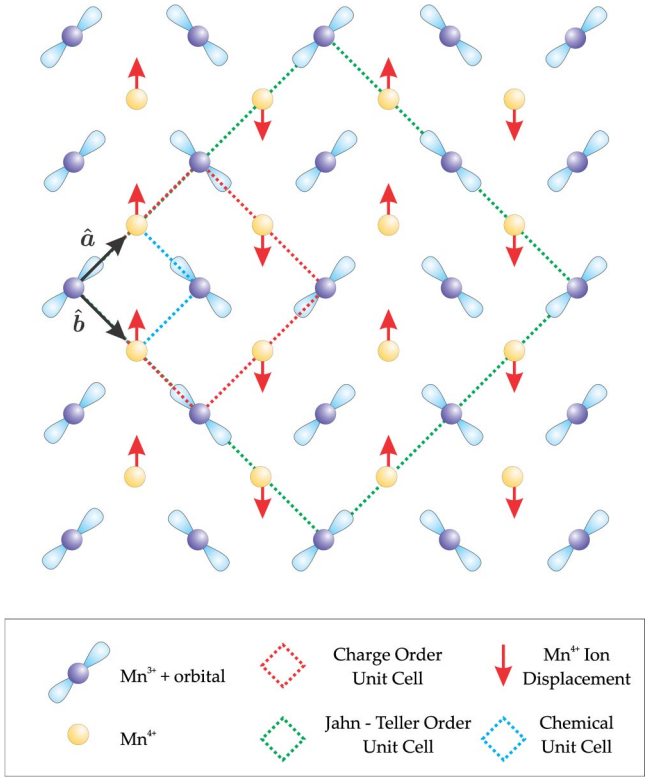

FIG. 2. Diagram showing a schematic of the charge, orbital, and cooperative Jahn-Teller order in the *a*-*b* plane in the bilayer.

(0.5, 0.5, 0) and the signal due to the orbital order at (0.25, 0.25, 0). In this paper we will clarify the correct positions of the charge and orbital order. We postulate that the modulation that occurs at (0.25, 0.25, 0) seen at high energy and using electron diffraction is caused by co-operative Jahn-Teller ordering on the Mn^{3+} ions, which consists of an elongation of certain Mn-O bonds. This elongation of the bond length causes the Mn^{4+} ions to move from their high-temperature position, which results in a lowering of the symmetry of the crystal structure. The charge order from the true Mn^{3+}/Mn^{4+} pattern occurs at a modulation of (0.5, 0.5, 0).

Here we report on a high-energy and resonant x-ray scattering study of charge and orbital ordering within the $La_{2-2x}Sr_{1+2x}Mn_2O_7$ system for the doping levels $x=0.5$ and $x=0.475$. The $x=0.475$ sample is of interest because it is very close to the 0.47 boundary below which the charge ordered state is not observed and has not been reported on by the previous x-ray measurements.[13,14] By observing the behavior of the charge ordered state in the $x=0.475$ sample and comparing the results with those from the $x=0.5$ sample, it is hoped to understand the charge ordered region of the phase diagram as shown in Fig. 3.

II. EXPERIMENTAL DETAILS

High-quality single-crystal samples of $La_{2-2x}Sr_{1+2x}Mn_2O_7$ with $x=0.5$ and 0.475 were grown using the floating-zone method at the University of Oxford. The $x=0.5$ and 0.475 samples had dimensions $6\times1.5\times0.5$ mm^3 and $6\times4\times1$ mm^3, respectively.

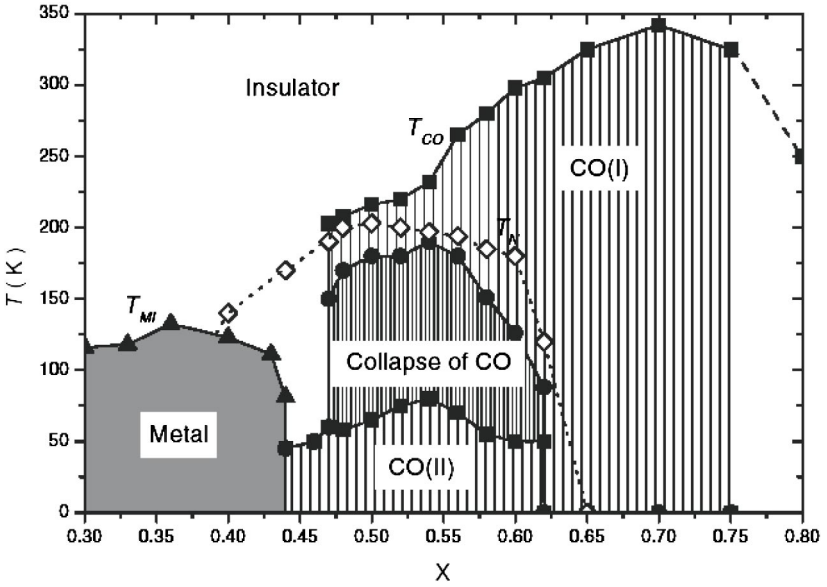

FIG. 3. The phase diagram of the bi-layer system as a function of temperature and doping concentration over the range $0.3<x<0.8$. The filled symbols show the transport data and the open symbols are from previously reported values taken from Ref. 15.

The high-energy x-ray studies were carried out at the Hamburger Synchrotronstralunglabour (HASYLAB) at DESY, Hamburg, on the high-energy wiggler beam line BW5.[16] The incident beam was monochromated using a graded $Si_{1-x}Ge_x$ crystal in transmission geometry. The sample, located in a closed cycle He cryostat with a temperature range from ~10 K to ~300 K was mounted in triple-axis geometry on a four-circle diffractometer. A similar graded $Si_{1-x}Ge_x$ crystal was used as an analyzer crystal and the scattered x rays were detected with a solid-state Ge detector. Both samples were mounted with the [110] and [001] directions lying within the diffraction plane.

The resonant x-ray scattering experiments were carried out on the XMaS beam line BM28 at the ESRF in Grenoble, France.[17] The incoming beam was monochromated by means of a constant exit double-bounce silicon (111) monochromator and focused using a pneumatically bent silicon mirror coated with rhodium. The sample was mounted on the 11-axis, 6-circle Huber diffractometer within a closed cycle He cryostat similar to that used at BW5. Measurements were undertaken in the vicinity of the manganese *K* edge, corresponding to an energy of 6.555 keV. Polarization analysis was provided by means of a copper (220) crystal diffracting close to its Brewster's angle. The incident beam was 93% plane polarized and the energy resolution ($\Delta E/E$) of the monochromator was 2 eV. All flight paths were evacuated to reduce the effects of absorption. The crystals were found to cleave naturally along the *a*-*b* plane, which resulted in the samples forming platelets with the [001] direction normal to the large surface. Due to the high absorption of the x rays, the measurements were undertaken in reflection geometry, which in turn placed the requirement that the scattering was performed with the [001] direction forming the on-axis direction.

III. RESULTS FROM $x=0.5$

A. High-energy diffraction

Initially measurements were undertaken on a sample of $La_{2-2x}Sr_{1+2x}Mn_2O_7$ with $x=0.5$, the same composition previously studied by Chatterji *et al.*[13] and Wakabashi *et al.*[14] After cooling the sample to 170 K, the temperature corresponding to the maximum in intensity from the previous studies, a search for superlattice reflections from both the Jahn-Teller order and charge order was undertaken.

Reflections of appreciable intensity were found, with the strongest being situated around the (1, 0, 5) Bragg reflection. Superlattice reflections were found with a modulation wave vector of $\vec{Q}=(-0.25,-0.25,0)$, which was consistent with the superlattice reflections found by Chatterji *et al.*[13] in their high-energy results. In addition, weaker superlattice reflections were also located at a modulation wave vector of $\vec{Q}=(-0.5,-0.5,0)$, not reported in the study of Chatterji *et al.*,[13] but observed by Wakabayashi *et al.*[14] We therefore propose that the reflections at $\vec{Q}=(-0.25,-0.25,0)$ are, in fact, due to a Jahn-Teller ordering with the charge ordering reflections appearing at $\vec{Q}=(-0.5,-0.5,0)$ consistent with the model presented earlier and the work of Wakabayashi *et al.* (see Fig. 2).

A systematic study of the superlattice reflections (0.75, −0.25, 5), the (1, 1, 5) reflection in the *Amam* cell, and (0.5, −0.5, 5), the (0, 1, 5) reflection in the *Amam* cell, corresponding to the Jahn-Teller and charge order, respectively, was undertaken. At 170 K, the peak intensities were measured to be 34.2×10^3 counts per second (cps) for the Jahn-Teller ordering and 1.2×10^3 cps for the charge ordering reflection. Upon cooling to 10 K, the superlattice reflections were found not to disappear, but had decreased in intensity appreciably. The peak intensities at 10 K were 5.1×10^3 cps for the Jahn-Teller order and 147 cps for the charge order.

The temperature dependence of the integrated intensity and width of the Jahn-Teller and charge order reflections were measured upon warming from 10 K. Scans were taken along the three principal directions in reciprocal space (*H*, *K*, and *L*) in triple-axis geometry. Data in all three directions were found to fit to a Lorentzian squared line shape. The results of these are shown in Figs. 4 and 5 for the Jahn-Teller (JT) order and charge order, respectively. The presence of the

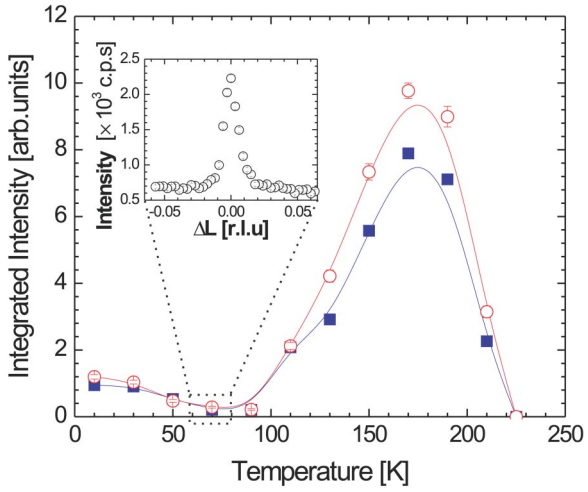

FIG. 4. Temperature dependence of the (0.75, −0.25, 5) Jahn-Teller distortion peak as measured in the H (solid squares) and K directions (open circles). The inset displays a scan through the Jahn-Teller superlattice reflection in the L direction at 70 K showing the nonzero intensity for the $x=0.5$ sample.

superlattice reflections from both the charge order and Jahn-Teller order indicates that contrary to the assumption of Wakabayashi *et al.*,[14] the charge order is not reentrant but exists at low temperature in a weaker state. We shall now consider the temperature dependence of the Jahn-Teller order upon warming from 10 K. Here it can be seen that upon warming the integrated intensity starts to fall, reaching a minimum at a temperature of 70 K. However, even at this temperature the reflection is easily observable, as indicated by the inset of Fig. 4, with a peak intensity of 1.57 $\times 10^3$ cps, after subtraction of the background. Upon further warming the integrated intensity stays constant until a temperature of 90 K, upon which the intensity starts to rapidly grow, reaching a maximum at a temperature of 170 K. Further warming causes the integrated intensity to fall again until it is not observable above background at a temperature of 225 K. The charge order reflection was found to display the same trend, as indicated by Fig. 5.

The inverse correlation length ξ^{-1} of the reflection was calculated by the following equation:

$$\xi_d^{-1}=\frac{2\pi}{d}w, \tag{1}$$

where w is the half-width at half maximum of the reflection and d is the lattice parameter along the direction of the reflection. Table I shows the inverse correlation length of the Jahn-Teller order at temperatures of 10 K and 170 K. Here no significant difference can be seen in the inverse correlation length at the two temperatures. In addition, the charge order was not found to display any change in inverse correlation length over the whole temperature range.

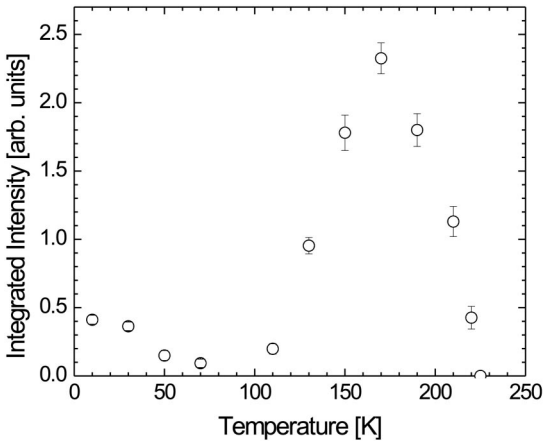

FIG. 5. Temperature dependence of the (0.5, −0.5, 5) charge order peak for the $x=0.5$ sample.

IV. RESULTS FROM $x=0.475$

A. Mn K-edge resonant x-ray scattering

The sample was cooled to 180 K, similar to the case for the $x=0.5$ sample, and a search was carried out for satellite reflections corresponding to the Jahn-Teller, charge, and orbital orders. Superlattice reflections were located at (0.5, 0.5, 10), (0.25, 0.25, 10), and (2.25, −0.25, 10). By polarization analysis of the scattered x-ray beam, the (0.5, 0.5, 10) and (2.25, −0.25, 10) reflections were found to be primarily σ' polarized (i.e., no rotation of the plane of polarization), whereas the (0.25, 0.25, 10) was found to be π' polarized, corresponding to a rotation of $\pi/2$ of the plane of polarization. The (0.25, 0.25, 10) reflection was found only to have appreciable intensity in the vicinity of the manganese K edge.

Let us first consider the case of the reflection located at (0.5, 0.5, 10). Such a resonance occurs due to the asymmetry between the resonant scattering factors $f'(\hbar\omega)$ and $f''(\hbar\omega)$ for the Mn^{3+} and Mn^{4+} species. The total scattering from a ion is given by

$$f(\vec{q},\hbar\omega)=f_0(\vec{q})+f'(\hbar\omega)+if''(\hbar\omega). \tag{2}$$

TABLE I. Inverse correlation lengths measured on the (0.75, −0.25,5) Jahn-Teller ordering peak at 10 K and 170 K.

	Inverse correlation length [$\times 10^{-3}$ Å^{-1}]		
Temperature	H	K	L
10 K	1.642±0.046	2.148±0.062	2.559±0.040
170 K	1.900±0.034	2.245±0.061	2.570±0.082
Ratio $\xi^{-1}_{10\,K}/\xi^{-1}_{170\,K}$	0.864	0.957	0.995

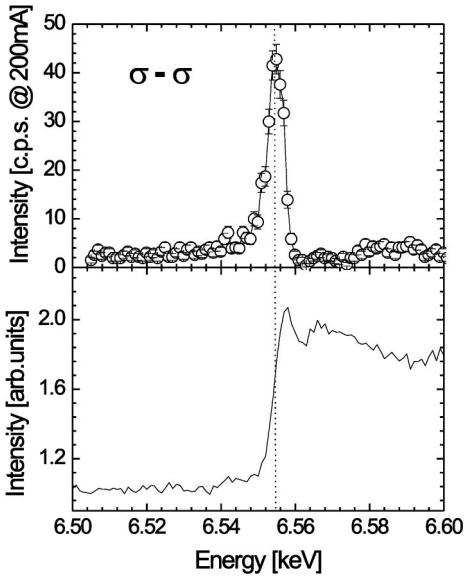

FIG. 6. Energy scan at constant $\vec{q}$ of the (0.5, 0.5, 10) charge order peak. The fluorescence spectrum measured on the sample is shown by the solid line confirming the location of the energy resonance in the $x=0.5$ sample.

For the charge order reflection, the total resonant scattering becomes

$$f(\vec{q},\hbar\omega)_{CO}=f'(\hbar\omega)_{3+}+if''(\hbar\omega)_{3+}-f'(\hbar\omega)_{4+} -if''(\hbar\omega)_{4+}+C, \quad (3)$$

where 3+ and 4+ denote the valence state of the manganese ion. The parameter C comes from the contribution due to the nonresonant scattering $[f^0(\hbar\omega)]$ and scattering due to asymmetry in the position of the oxygen ions. Due to the effects of chemical shift, the edge positions for the Mn^{3+} and Mn^{4+} ions will be altered, resulting in an increase in the contrast between the Mn^{3+} and Mn^{4+} ions between the energy of each absorption edge from the initial off-resonant difference of less than one electron. The resonance observed in Fig. 6 is consistent with such a model, and it is thus attributed to be due to the charge order. The resonance was observed to occur at the *K*-edge position of 6.556 keV as indicated by the fluorescence spectrum shown in the lower panel of Fig. 6 and the polarization was found to be unrotated.

The reflection at (2.25, −0.25, 10), of which the energy dependence is shown in Fig. 7, shows behavior that would be expected from a structural modulation caused by the motion of the Mn^{4+} species only (see Fig. 2) as mentioned previously for the Jahn-Teller order. Such a dip in the intensity at the absorption edge is due to the increased absorption post edge, which reduces the probed sample volume, in turn reducing the signal.

Finally, the reflection at (0.25, 0.25, 10), which behaved differently to the previous reflections was found to have a final polarization state rotated $\pi/2$ from the incident beam, in addition to having only appreciable intensity at the *K* edge (see Fig. 8). Similar results were found on the (0.25, −0.25, 10) position. This is consistent with the origin of the

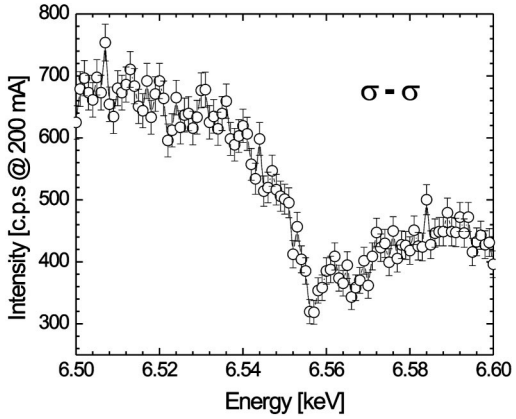

FIG. 7. Energy scan at constant wave vector corresponding to the (2.25, −0.25, 10) co-operative Jahn-Teller distortion reflection in the $x=0.5$ sample.

reflection being from the orbital order, caused by a splitting of the $4p$ energy levels from the ordering of the $3d$ orbitals. The theory behind such a resonance has not clearly been determined, with two possible models. The first one has the $4p$ states being split due to a hybridization of the Mn($3d$)-O($2p$) and O($2p$)-Mn($4p$) states.[18] Whilst the second one has the $4p$ states split due to Coulomb coupling between the $4p$ and $3d$ state,[18] which will cause an increase in the $4p$ levels lying parallel to the extension of the $3d$ orbital and reducing the energy perpendicular to such extension. With resonant x-ray scattering at the *K* edge it is impossible to separate the two models presented above, but both are indicative of an orbital ordering process.

B. High-energy x-ray scattering

As in the case for the $x=0.5$ sample, the sample with $x=0.475$ was studied using the high-energy x-ray scattering. The sample was mounted with the [110] and [001] direc-

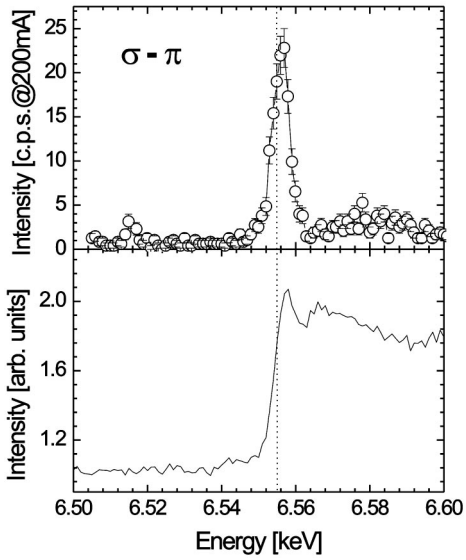

FIG. 8. Energy scan at constant wave vector corresponding to the (0.25, 0.25, 10) orbital order reflection in the $x=0.5$ sample.

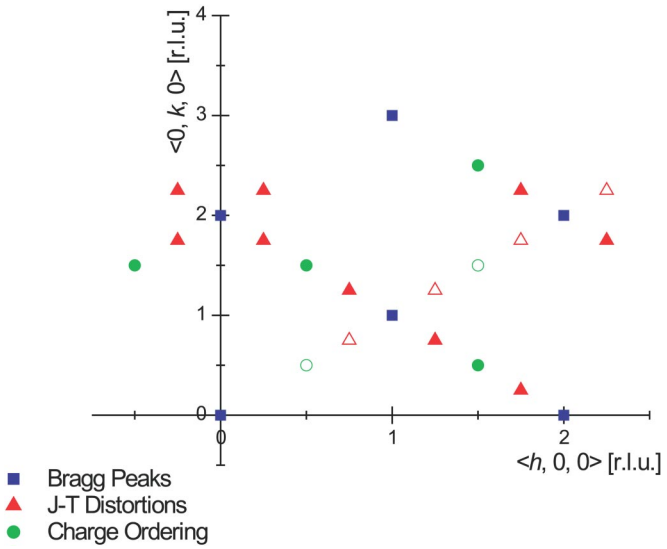

FIG. 9. Location of the Bragg peaks (squares), charge ordering (circles), and cooperative Jahn-Teller distortions (triangles). Closed and open symbols indicate locations where strong or weak reflections were located, respectively, found in the $x=0.475$ sample.

tions lying within the diffraction plane. Triple-axis measurements were carried out in the same manner described previously for the $x=0.5$ sample.

The sample was cooled to 180 K, which corresponds to the maximum in intensity observed in previous studies. Strong superlattice reflections were located around the the (1, 1, 0) Bragg peak with modulations of (0.25, −0.25, 0) and (−0.25, 0.25, 0). Also present were weak reflections at modulations of (0.25, 0.25, 0) and (−0.25, −0.25, 0). In addition, strong reflections were found with a modulation of (0.5, −0.5, 0) with weak reflections again at (−0.5, 0.5, 0). We attribute these to be due to the Jahn-Teller order and charge order, respectively, in agreement with the resonant scattering data presented above. A systematic study was undertaken to observe peaks in the [100]/[010] plane of reciprocal space. The results are shown in Fig. 9. Apparent from this data is that strong reflections were seen only along the [110] direction, with weaker reflections along the 90° rotated [110] direction.

At 180 K, the (1.75, 0.25, 0) superlattice reflection was measured along the three principal directions, *H*, *K*, and *L*. The data were found to fit best to a Gaussian line shape along the *H* direction, with the *K* and *L* directions displaying a Lorentzian squared line shape. Fits to these data are shown in Fig. 10. The sample was then further cooled to ~10 K and the intensity of the superlattice reflections corresponding to the Jahn-Teller order were found to decrease, but were still observable above background. Scans in *H*, *K*, and *L* were repeated at this new temperature. Table II shows a comparison of the inverse correlation lengths calculated using Eq. (1), at 180 K and 10 K. There is a clear broadening in the peaks at low temperature, especially in the *L* direction; however, along the *H* direction the broadening is not as apparent.

The Jahn-Teller ordering superlattice reflection was studied as a function of temperature from 10 K. Fig. 11 shows the integrated intensity, wave vector, and inverse correlation length over the temperature region 10–240 K. For the integrated intensity, we can see from the top panel of Fig. 11 that the intensity of the Jahn-Teller distortion stays constant until 100 K, at which point it starts to increase. A maximum is reached at 180 K, at which point the integrated intensity has increased by a factor of ~6. Upon further warming, the integrated intensity starts to decrease until 220 K, where the peak was barely observable above background. We now turn to the inverse correlation length, displayed in the bottom panel of Fig. 11. In this case the inverse correlation length stays constant until ~100 K, at which point it starts to fall, indicating an increase in correlation until the temperature again reaches 220 K, where the inverse correlation length starts to increase. From these data it is possible to see that there exist three main temperature regions. In the range $10\ \text{K} \leqslant T \leqslant 140\ \text{K}$ (region *I* in Fig. 11) the Jahn-Teller order exists in a low-intensity, less correlated region than in the region $140\ \text{K} < T \leqslant 210\ \text{K}$ (region *II* in Fig. 11), where the Jahn-Teller distortion is large, which is more correlated than at low temperature. Above 220 K (region *III*) there is no detectable Jahn-Teller order. The integrated intensity is proportional to the amplitude squared of the electron density, the superlattice reflections arise due to the movement of the Mn^{4+} ions and the displacement of the oxygen ions due to the elongation of the Mn-O bonds caused by the Jahn-Teller effect; and therefore as the Mn-O bond length increases, the Mn^{4+} ions will be further moved, causing an increase in the asymmetry of the electron density. This will, in turn, cause an increase in the integrated intensity. We can therefore conclude that in region *I* the magnitude of the Jahn-Teller distortions (i.e., the Mn-O bond length) is less than in region *II*. In addition, in region *I* the correlation of the cooperative ordering of the Mn-O bond length elongation is less than in region *II*. An alternative explanation for the nature of the reentrant charge behavior is a movement of the holes as a

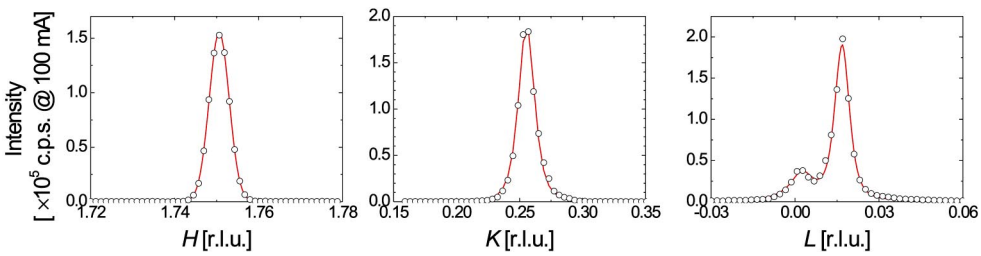

FIG. 10. Scan through the *H* (left), *K* (center), and *L* (right) directions of the (1.75, 0.25, 0) JT order peak at $T=180$ K. The solid line is a fit to the experimental data (see text for details) in the $x=0.475$ sample.

TABLE II. Inverse correlation lengths measured on the (1.75, 0.25, 0) Jahn-Teller ordering peak at 10 K and 180 K.

	Inverse correlation length [$\times 10^{-3}$ Å^{-1}]		
Temperature	H	K	L
10 K	2.677±0.06	13.69±0.03	6.59±0.02
180 K	1.934±0.007	4.690±0.008	0.3977±0.002
Ratio $\xi^{-1}_{10\ \mathrm{K}}/\xi^{-1}_{180\ \mathrm{K}}$	1.384	2.919	16.57

function of temperature. At high temperatures (region *II*), the holes are believed to reside at the positions of the manganese ions. At low temperatures a movement of the holes towards the oxygen positions would cause a reduction in the Mn^{4+} Jahn-Teller displacements, and thus a reduction in the scattered intensity. Physically, this corresponds to a shift of the e_g electron density (localized at the Mn^{3+} sites) towards the oxygen sites, and thus delocalized between Mn pairs.

In addition to the integrated intensity and inverse correlation length, the wave vector (position) was measured along the ⟨100⟩ direction as a function of temperature, the results of which are displayed in the central panel of Fig. 11. Here we can see that in region *I* the Jahn-Teller order exists at an incommensurate value, but, upon warming at the boundary into region *II*, the wave vector locks into a commensurate value of 1.75. The incommensurability corresponds to a value $\varepsilon=0.004$ r.l.u., which suggests a long period modulation of the Jahn-Teller distortion. No change in position of the wave vector along the *K* or *L* direction was observed, due to the larger peak width in these directions. Charge ordering in the 3D perovskites such as $Pr_{0.5}Ca_xSr_{0.5-x}MnO_3$ develops by particular steps, suggesting that the observed incommensurability is caused by quasiperiodic defects, that is, discommensurations.[19] However, the very small value of the incommensurability would suggest such discommensurations would be separated by lengths approaching the domain size, hence such deviations could be due to an effect of domain boundaries. Previous studies by Radaelli *et al.*[20] using powder neutron diffraction on samples of $La_{1-x}Ca_xMnO_3$ have also observed an incommensurability of the Jahn-Teller order, however, no ''lock-in'' behavior was reported.

Similar measurements were also carried out on the charge order. No charge order was detectable at 10 K, in contrast to the $x=0.5$ sample. However, at 120 K, superlattice reflections were visible above the background and the temperature dependence in the region 120–210 K of the (1.5, 0.5, 0) charge order reflection was studied, with the results being shown in Fig. 12. At the maximum in intensity at 180 K, the charge order was found to be ~50 times weaker than the corresponding Jahn-Teller order. This is the first observation of charge ordering reflections for any composition other than $x=0.5$. Previous synchrotron x-ray and neutron-powder-diffraction studies did not observe charge ordering except for $x=0.5$.[21]

Within this temperature range the charge order is found to display the same variation as the Jahn-Teller order with temperature, maximizing at the same temperature of 180 K. The inverse correlation length along the three principal directions

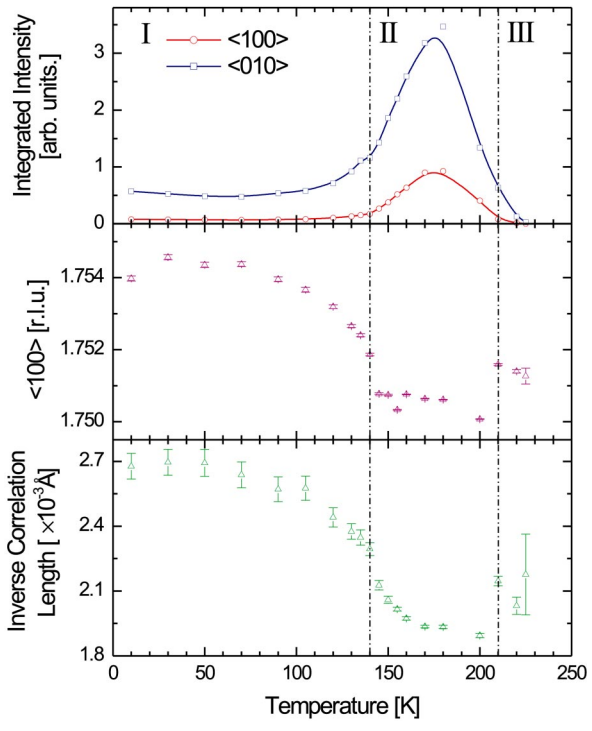

FIG. 11. Integrated intensity, position and inverse correlation length of the (1.75, 0.25, 0) Jahn-Teller reflection as a function of temperature in the $x=0.475$ sample. In the top panel, open circle and square symbols represent the integrated area measured in the *H* and *K* directions, respectively.

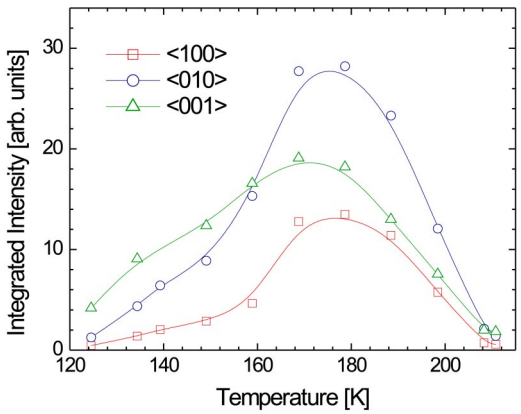

FIG. 12. Integrated intensity in the *H* (squares), *K* (circles), and *L* (triangles) directions of the charge order reflection (1.5, 0.5, 0) in the $x=0.475$ sample. Solid lines are a guide to eye.

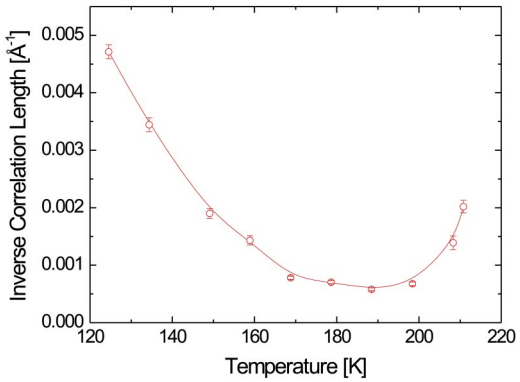

FIG. 13. Inverse correlation length as a function of temperature in the L direction for the (1.5, 0.5, 0) charge order reflection in the $x=0.475$ sample.

in reciprocal space was calculated using Eq. (1). No variation with temperature was observed over the whole range studied along the H and K directions. However, along the L direction a distinct variation was observed. Figure 13 shows the inverse correlation length as a function of temperature. Here a broadening at low temperature is apparent, which indicates that at low temperature the charge ordering is becoming more two dimensional in nature.

The absence of the charge order reflection at 10 K, in contrast to the $x=0.5$ sample, does not suggest that the $x=0.475$ sample is not charge ordered. The presence of Jahn-Teller order at the modulation wave vector $\vec{Q}=(0.25, 0.25,0)$ relies upon the model of a ''checkerboard- like'' charge ordering as displayed schematically in Fig. 2. In the absence of any charge ordering, the Jahn-Teller ordering would not appear at this wave vector. Therefore we propose that the $x=0.475$ sample is charge ordered at low temperatures, but it is not of sufficient intensity to observe above the experimental background.

Finally, we carried out high-resolution measurements on the Bragg peaks at station 16.3 at the SRS, Daresbury Laboratory, UK, with an incident wavelength of 1 Å. A silicon (111) analyzer was used to provide high-resolution measurements. The temperature dependence of the wave vector (position), width, and intensity of the Bragg peaks was collected on the same sample as studied with the high-energy experiments for the (1, −1, 16) Bragg reflection. No significant change in wave vector or integrated intensity was observed in any of the principal reciprocal space directions over the temperature range 10 K$\leqslant T\leqslant$300 K. However, a clear increase in the inverse correlation length along the L direction can be seen, in agreement with Wakabayashi *et al.*[14] These data are shown in Fig. 14.

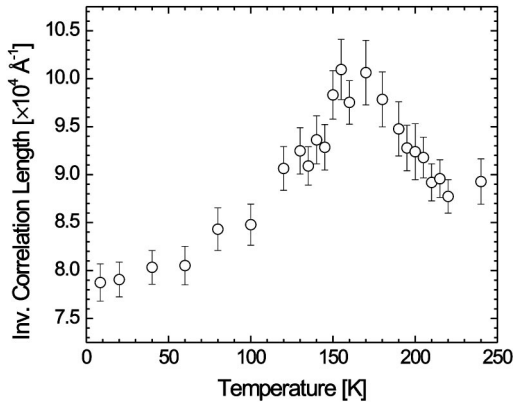

FIG. 14. Temperature dependence of the inverse correlation length of the (1, −1, 16) Bragg peak in the L direction in the $x=0.475$ sample.

We propose that the increase in inverse correlation length occurs due to the presence of charge and Jahn-Teller order, which causes strains within the lattice, the maximum of the strain coincides with the temperature of the maximum Jahn–Teller distortion.

V. CONCLUSIONS

In summary, we have used high-energy x-ray scattering along with resonant x-ray scattering to investigate the Jahn-Teller, charge, and orbital order in the bilayer manganite $La_{2-2x}Sr_{1+2x}Mn_2O_7$ with $x=0.5$ and 0.475.

These studies have confirmed the correct modulation wave vector for the charge, orbital, and Jahn-Teller order as $\vec{Q}_{CO}=(0.5, 0.5, 0)$, $\vec{Q}_{OO}=(0.25, 0.25, 0)$, and $\vec{Q}_{J-T}=(0.25, 0.25, 0)$, respectively. This is in agreement with the resonant x-ray scattering studies of Wakabayashi *et al.*,[14] but is in contrast with the results of Chatterji *et al.* We propose that the charge order reflections measured by Chatterji *et al.* are, in fact, due to cooperative Jahn-Teller order. The resonant scattering data presented here using polarization analysis on the $x=0.475$ sample confirms the origin of the scattering at each of these wave vectors.

Work previous to this report had suggested that the charge and orbitally ordered state is reentrant in behavior. However, the results here on both the $x=0.5$ and $x=0.475$ show that the ordered state exists down to the lowest temperature of these measurements, ~10 K. In fact, the previous transition (whereby the ordered state was seen to disappear), is, in fact, only a reduction in intensity of the ordering, with an additional reduction in correlation in the $x=0.475$ sample.

There are clear differences between the ordered states in the $x=0.5$ and $x=0.475$ systems. First, in the $x=0.5$ sample the correlation of the Jahn-Teller and charge ordering, indicated by the inverse correlation lengths, does not change over the whole temperature range, at which there is sufficient intensity to observe the superlattice reflection. However, in the $x=0.475$ sample there are three clear temperature regions; at high temperatures there is no Jahn-Teller order, the second one occurs at moderately high temperatures where the Jahn-Teller order and charge order are highly correlated and intense, and third at lower temperatures where the Jahn-Teller order is weak and less correlated than at higher temperatures. In addition, the temperature variation along the L direction for the charge order suggests that at low temperature the charge order is becoming more two-dimensional-like. The presence of Jahn-Teller order indicates that the charge order is still present. In the low-temperature region of the $x=0.475$ sample, the Jahn-Teller order is found to be incommensurate with a transition at 140 K into a commensurate phase. Such a lock-in behavior of the Jahn-Teller order

was not seen in the $x=0.5$ sample. Unlike the $x=0.475$ sample, the intensity of the Jahn-Teller and charge order in the $x=0.5$ sample is found to be greater at 10 K than at 70 K. Upon warming, a reduction in intensity before the dramatic increase into the higher temperature region is observed. Such behavior has been recently theoretically predicted through polaron bandwidth calculations by Yuan and Thalmeier.[22]

ACKNOWLEDGMENTS

The authors would like to thank Steve Collins of the SRS, CLRC Daresbury Laboratory, UK, for his assistance during the measurements at station 16.3. The work at the HASYLAB was supported by IHP Contract No. HPRI-CT-1999-00040 of the European Commission. The authors are also grateful to the XMaS beam line team of D. F. Paul, D. Mannix, and P. Thompson for their invaluable assistance, to S. Beaufoy and J. Kervin for additional support, and EPSRC for financial support. S.B.W. and P.D.S. would like to thank the EPSRC for financial support, and P.D.H. would like to thank the University of Durham, Sir James Knott Foundation for financial support and S.B.W. and P.D.S. thank EPSRC for the same.

*Present address: European Commission, Joint Research Center, Institute for Transuranium Elements (ITU), Hermann von Helmholtz-Platz 1, 76344 Eggenstein-Leopoldshafen, Germany, and European Synchrotron Radiation Facility, Boîte Postale 220, F-38043 Grenoble Cedex, France.

†Electronic address: p.d.hatton@durham.ac.uk

[1] J. Tranquada, B. Sternlieb, J. Axe, Y. Nakamura, and S. Uchida, Nature (London) **375**, 561 (1995).

[2] A.J. Millis, Phys. Rev. B **53**, 8434 (1996).

[3] Y. Murakami, H. Kawada, H. Kawata, M. Tanaka, T. Arima, Y. Moritomo, and Y. Tokura, Phys. Rev. Lett. **80**, 1932 (1998).

[4] Y. Murakami *et al.*, Phys. Rev. Lett. **81**, 582 (1998).

[5] Y. Moritomo, Y. Tomioka, A. Asamitsu, Y. Tokura, and Y. Matsui, Phys. Rev. B **51**, 3297 (1995).

[6] A. Urushibara, Y. Moritomo, T. Arima, A. Asamitsu, G. Kido, and Y. Tokura, Phys. Rev. B **51**, 14 103 (1995).

[7] Y. Moritomo, A. Asamitsu, H. Kuwahara, and Y. Tokura, Nature (London) **380**, 141 (1996).

[8] J. Goodenough, Phys. Rev. **100**, 564 (1955).

[9] K. Nakamura, A. Arima, A. Nakazawa, Y. Wakabayashi, and Y. Murakami, Phys. Rev. B **60**, 2425 (1999).

[10] M.v. Zimmermann, J.P. Hill, D. Gibbs, M. Blume, D. Casa, B. Keimer, Y. Murakami, Y. Tomioka, and Y. Tokura, Phys. Rev. Lett. **83**, 4872 (1999).

[11] J.Q. Li, Y. Matsui, T. Kimura, and Y. Tokura, Phys. Rev. B **57**, R3205 (1998).

[12] T. Kimura, R. Kumai, Y. Tokura, J. Li, and Y. Matsui, Phys. Rev. B **58**, 11 081 (1998).

[13] T. Chatterji, G.J. McIntyre, W. Caliebe, R. Suryanarayanan, G. Dhalenne, and A. Revcolevschi, Phys. Rev. B **61**, 570 (2000).

[14] Y. Wakabayashi, Y. Murakami, I. Koyama, T. Kimura, Y. Tokura, Y. Moritomo, K. Hirota, and Y. Endoh, J. Phys. Soc. Jpn. **69**, 2731 (1999).

[15] J. Dho, W.S. Kim, H.S. Choi, E.O. Chi, and N.H. Hur, J. Phys.: Condens. Matter **13**, 3655 (2001).

[16] R. Bouchard, R. Hupfeld, D. Lippmann, T. Neuefeind, H.F. Poulsen, U. Rutt, T. Schmidt, J.R. Schneider, J. Sussenbach, and M. von Zimmermann, J. Synchrotron Radiat. **5**, 90 (1998).

[17] S.D. Brown *et al.*, J. Synchrotron Radiat. **8**, 1172 (2001).

[18] S. Ishihara and S. Maekawa, Phys. Rev. B **58**, 13 442 (1998).

[19] Z. Jirák, F. Damay, M. Hervieu, C. Martin, B. Raveau, G. André, and F. Boureé, Phys. Rev. B **61**, 1181 (2000).

[20] P. Radaelli, D. Cox, M. Marezio, and S.-W. Cheong, Phys. Rev. B **55**, 3015 (1997).

[21] C.D. Ling, J.E. Millburn, J.F. Mitchell, D.N. Argyriou, J. Linton, and H.N. Bordallo, Phys. Rev. B **62**, 15 096 (2000).

[22] Q. Yuan and P. Thalmeier, Phys. Rev. Lett. **83**, 3502 (1999).